Time-Resolved Polarization Imaging By Pump-Probe (Stimulated Emission) Fluorescence Microscopy

Ch. Buehler,* C. Y. Dong,† P. T. C. So,† T. French,‡ and E. Gratton§

*Novartis Pharma AG, Pharma Research, CTA, LFU/NAT S-360.4.16, CH-4002 Basel, Switzerland; †Department of Mechanical Engineering, Massachusetts Institute of Technology, Cambridge, Massachusetts 02139 USA; ‡LJL Biosystems, Sunnyvale, California 94089 USA; and §Laboratory for Fluorescence Dynamics, Department of Physics, University of Illinois at Urbana-Champaign, Urbana, Illinois 61801 USA

ABSTRACT We report the application of pump-probe fluorescence microscopy in time-resolved polarization imaging. We derived the equations governing the pump-probe stimulated emission process and characterized the pump and probe laser power levels for signal saturation. Our emphasis is to use this novel methodology to image polarization properties of fluorophores across entire cells. As a feasibility study, we imaged a 15-μm orange latex sphere and found that there is depolarization that is possibly due to energy transfer among fluorescent molecules inside the sphere. We also imaged a mouse fibroblast labeled with CellTracker Orange CMTMR (5-(and-6)-(((4-chloromethyl)benzoyl)amino)tetramethyl-rhodamine). We observed that Orange CMTMR complexed with gluthathione rotates fast, indicating the relatively low fluid-phase viscosity of the cytoplasmic microenvironment as seen by Orange CMTMR. The measured rotational correlation time ranged from ~30 to ~150 ps. This work demonstrates the effectiveness of stimulated emission measurements in acquiring high-resolution, time-resolved polarization information across the entire cell.

INTRODUCTION

Fluorescence microscopy in biology

Fluorescence microscopy allows imaging of specific cellular microstructures in great detail. There have been different developments aimed at improving the spatial resolution in microscopic imaging by reducing off-focal fluorescence. In particular, confocal microscopy (Wilson and Sheppard, 1984; Wilson, 1990) improves the spatial resolution to the submicron range. In two-photon fluorescence microscopy, similar spatial resolution and off-focal fluorescence reduction can be achieved by inducing nonlinear excitation of the fluorescent sample (Denk et al., 1990). Compared to confocal microscopy, the localization of excitation to the focal volume attained by two-photon excitation significantly reduces photobleaching in off-focal regions. Although spatial resolution much less than the wavelength of light can be obtained with near-field microscopy (Betzig et al., 1993), this technique is limited to surface studies. Recently, pump-probe (stimulated emission) microscopy has been demonstrated to provide images with spatial resolution comparable to that of confocal microscopy and at potentially very high temporal resolution (Dong et al., 1995). The main focus of this work is to extend the pump-probe (stimulated emission) method to time-resolved anisotropy studies in microscopy. Our objective is to obtain image sections based on the rotational correlation time of a probe in a cell and to accurately determine the characteristic time of the anisotropy decay.

Received for publication 31 March 1999 and in final form 6 April 2000.

Address reprint requests to Dr. Chen-Yuan Dong, Massachusetts Institute of Technology, Room 3-335, 77 Massachusetts Ave., Cambridge, MA 02139. Tel.: 617-253-2223; Fax: 617-258-9346; E-mail: cdong@mit.edu.

0006-3495/00/07/536/14 $2.00

Lifetime-resolved fluorescence microscopy

In fluorescence microscopy, lifetime-resolved images can provide insights into functionally important processes in biological systems. Dynamics of the chromophores in their local environments can be characterized, and this can help to elucidate the functioning of cellular components at the molecular level. Many applications of fluorescence lifetime imaging have been demonstrated. Important cellular information such as calcium concentration or cytoplasm matrix viscosity have been obtained by lifetime-resolved methods (Dix and Verkman, 1990; Keating and Wensel, 1990; Kao et al., 1993). Measurements of the autofluorescence lifetime have been used to monitor the mechanism responsible for cell damage due to UVA exposure (Schneckenburger et al., 1992; Schneckenburger and Koenig, 1992; Koenig and Schneckenburger, 1994). The fluorescence lifetime has also been used to assess antigen-processing stages in mouse macrophage cells (Voss, 1990). Furthermore, the spatial distribution of chromophores with similar emission spectra but different lifetimes provides a new contrast mechanism (Draaijer et al., 1995). Fluorescence lifetime-resolved studies have also been successfully conducted in confocal (Morgan et al., 1991; Buurman et al., 1992) and two-photon (Piston et al., 1992; So et al., 1996) scanning microscopy.

Cytoplasmic viscosity of cells

Various fluorescence techniques have been used to probe the (micro)viscosity of cytoplasm. Picosecond rotation of small fluorophores has been studied to estimate fluid-phase viscosity in the cell cytosol (Periasamy et al., 1991; Fushimi and Verkman, 1991). Recently, cytoplasmic viscosity has

been probed, using the diffusion and rotation of the green fluorescent protein (Swaminathan et al., 1997). All of these studies are essentially single point measurements inside cells, and they show that for small molecules, the viscosity of cytoplasm relative to that of water is between ~1 and 3. In our approach, we obtain time-resolved polarization images of a cytoplasmic probe throughout the cell. Imaging the entire cytoplasm may reveal the structural heterogeneity that exists inside a cell.

Lifetime and polarization measurements in the frequency domain

Time-resolved measurements in the frequency domain are performed by means of modulated light sources (Spencer and Weber, 1969; Gratton and Limkeman, 1983). For sinusoidal excitation at modulation frequency $\nu = \omega/2\pi$ and modulation m_e, the spatial ($\vec{r}$) and temporal (t) distribution of the excitation photon flux $I(\vec{r}, t)$ can be written as $I(\vec{r}, t) = I(\vec{r})[1 + m_e \sin(\omega t)]$. The number density of excited-state molecules $N(\vec{r}, t)$ of fluorophores with a single lifetime τ obeys the differential equation

$$\frac{dN(\vec{r}, t)}{dt} = -\frac{1}{\tau} N(\vec{r}, t) + \sigma I(\vec{r}, t)[c - N(\vec{r}, t)] \quad (1)$$

where σ is the molecular absorption cross section, and $\sigma I(\vec{r}, t)[c - N(\vec{r}, t)]$ denotes the number of ground-state molecules actually being excited by the light source. The total fluorophore concentration c is assumed to be constant. To the first order in which only a small fraction of molecules are excited, the fluorescence response $F(\vec{r}, t)$ is at the same modulation frequency as the excitation light but is demodulated and phase shifted:

$$F(\vec{r}, t) \propto I(\vec{r})[1 + m' \sin(\omega t + \phi)] \quad (2)$$

where m' denotes the modulation of the fluorescence response and ϕ is its phase shift with respect to the excitation light. By measuring either the phase shift ϕ or the demodulation $m = m'/m_e$, the fluorescence lifetime can be determined:

$$\tan(\phi) = \omega\tau_p \quad \text{and} \quad m = \frac{1}{\sqrt{1 + \omega^2\tau_m^2}} \quad (3)$$

where τ_p and τ_m denote the phase and modulation lifetimes, respectively. More complex excitation modulation functions, such as a laser pulse train, can be represented as a superposition of Fourier components. The fluorescence signal can then be represented as the sum of the response to each Fourier component (Spencer and Weber, 1969; Gratton and Limkeman, 1983; Gratton et al., 1984; Alcala and Gratton, 1985; Lakowicz, 1999).

Time-resolved anisotropy studies are performed by measuring the fluorescence parallel and perpendicular to the excitation polarization. For linearly polarized δ-pulse excitation, the parallel ($\parallel$) and perpendicular ($\perp$) components of the fluorescence decay are given by

$$i_\parallel(t) = \tfrac{1}{3} I(t)(1 + 2r(t)) \quad (4)$$

$$i_\perp(t) = \tfrac{1}{3} I(t)(1 - r(t)) \quad (5)$$

where $I(t)$ and $r(t)$ are the fluorescence and anisotropy decays, respectively. For an isotropic rotator, the anisotropy decay is given by

$$r(t) = r_0 e^{-(t/\Phi)} \quad (6)$$

where Φ is the rotational correlation time and r_0 is the initial anisotropy.

In the frequency domain the anisotropy is determined by measuring the frequency response of the differential phase $\Delta\phi = \phi_\perp - \phi_\parallel$ and modulation ratio Y between the parallel and perpendicular fluorescence signals. For an isotropic rotator, the differential phase $\Delta\phi$ and the (squared) modulation ratio Y^2 are given by

$$\Delta_\phi = \frac{3\omega R}{(k^2 + \omega^2)(1 + r - 2r^2) + R(R + 2k + kr)} \quad (7)$$

$$Y^2 = \frac{[k + 6R/(1 - r)]^2 + \omega^2}{[k + 6R/(1 + 2r)]^2 + \omega^2} \quad (8)$$

where r and R are the intrinsic anisotropy and the rotational rate, respectively, and k is the fluorescence decay rate. Note that R is the inverse of the rotational correlation time, i.e., $R = 1/\Phi$, and correspondingly, the fluorescence decay rate k is the inverse of the fluorescence lifetime τ, i.e., $k = 1/\tau$ (Gratton and Limkeman, 1983; Gratton et al., 1984; Alcala and Gratton, 1985; Lakowicz, 1999).

PUMP-PROBE FLUORESCENCE MICROSCOPY

Overview of pump-probe techniques

Pump-probe spectroscopy has been applied successfully to the investigation of ultrafast processes in biology, chemistry, and condensed matter. The temporal evolution of the process can be studied by varying the timing between the pump and probe pulses (Evans, 1989; Fleming, 1986; Lytle et al., 1985). A common approach is to excite the sample with a strong pulse of light (pump) and to sample the ground-state population with a weak pulse of light (probe). The temporal separation between these pulses is typically controlled by means of a mechanical delay line that allows fine control of the laser beams' optical paths. The ultimate temporal resolution of this type of pump-probe spectroscopy is determined by the pulse width of the laser. In the visible and near-IR wavelength ranges, the duration of light pulses is around a few femtoseconds (10^{-15}s) (Zhou et al., 1994; Xu et al., 1996; Christov et al., 1996). Ultrafast phenomena in many biological systems, including photo-

synthetic reaction centers, rhodopsin, and heme proteins, have been studied (Hochstrasser and Johnson, 1988).

An alternative method in pump-probe techniques is the asynchronous sampling version first proposed by the Lytle group (Elzinga et al., 1987). In this approach, two pulsed laser beams with different repetition rates are focused on the same spot in the sample to induce the pump-probe effect. The difference in repetition rates introduces a variable delay between the pump and probe pulses. The effect of this delay is to repeatedly sample the excited-state population of the molecules at consecutive time intervals after the pump laser pulses. A frequency domain analysis of the pump-probe signal generated in this manner shows that the (high-) frequency components of the fluorescence signal are shifted to the lasers' cross-correlation frequency and its harmonics. These frequency components can be analyzed to obtain time-resolved information. Harmonic content can be explored in excess of 12 GHz (Berland et al., 1992). Instead of sampling the transient absorption of the probe pulse, researchers can choose its wavelength to induce stimulated emission from the excited-state population. The stimulated emission approach has been demonstrated in spectroscopic studies (Lakowicz et al., 1994; Kusba et al., 1994; Adachi et al., 1995).

Imaging microscopy based on the asynchronous sampling technique offers several advantages over the equivalent technique that uses a mechanical delay line. To acquire time-resolved images by means of a mechanical delay line, either all of the fluorescence properties are measured in one pixel by running one laser beam through a series of time delays before moving to the next pixel, or the entire image is scanned at one particular time delay and consecutively repeated for all delay times, yielding a corresponding series of time slice images. Within an image acquisition time of 60 s, 30 time slice images at most can be recorded, because it takes ~2 s to scan an image of 256 × 256 pixels (cf. section Scanning Optics). With respect to frequency domain, this is equivalent to acquiring 15 harmonics of the fluorescence signal in each pixel. To measure 15 harmonics in one pixel at once, the time delay has to be switched 30 times within the pixel dwell time of ~1 ms, which is not mechanically feasible.

With the asynchronous sampling technique, 15 harmonics can easily be recorded at once within the 1-ms pixel dwell time, assuming a corresponding base cross-correlation frequency of 1 kHz and a moderate signal digitization rate of 30 kHz. Hence, by simply increasing the digitization rate, the asynchronous sampling technique allows us to retrieve more harmonic components of the fluorescence signal than the mechanical delay line approach within the given image acquisition time of 60 s. Furthermore, if the cross-correlation frequency is also increased, the image acquisition time can be reduced without losing harmonic information. However, the major advantage in using a mechanical delay line to perform pump-probe experiments is in the autocorrelation capability of the laser pulses. In this setup, the jitter between the pump and probe pulses is greatly reduced, resulting in improved temporal resolution.

Principle of the pump-probe stimulated emission technique

The basic principle of the stimulated emission technique is illustrated in Fig. 1. The beams of two pulsed lasers are focused onto a common volume inside the specimen. The pulse repetition rates of the two lasers are offset slightly, and their wavelengths are chosen such that the pump beam excites the chromophores under study and the probe beam induces stimulated emission. The optical modulation of the excited-state population by the probe pulses results in a heterodyning of the fluorescence signal, i.e., the Fourier spectrum of the fluorescence decay is translated to the cross-correlation frequency range. The high harmonic content of pulsed lasers (THz range for femtosecond lasers) allows the acquisition of multiple harmonics of the decay spectrum at once. The fluorescence signal containing the cross-correlation harmonics can be isolated by means of optical filtering, because the emission is at wavelengths different from those of both excitation and stimulated emissions.

The timing diagram shown in Fig. 2 further illustrates the principle of the pump-probe (stimulated emission) technique. The pulse train of the pump laser periodically excites

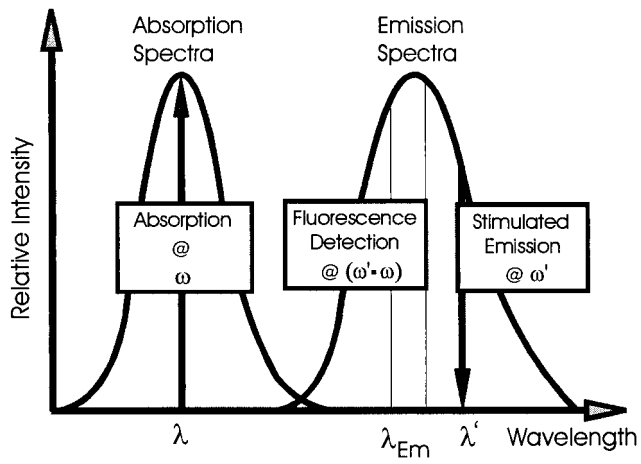

FIGURE 1 Principles of the pump-probe (stimulated emission) fluorescence technique. The sample population is excited by an intensity-modulated pump laser tuned in its wavelength λ to the corresponding molecular absorption band. The modulation frequency of the pump beam intensity is $\nu = \omega/2\pi$. The stimulated emission process is induced by the probe laser beam set to a wavelength λ′ within the fluorophores' emission spectrum. The probe beam intensity is slightly offset in its modulation frequency at $\nu' = \omega'/2\pi$. The fluorescence emission is detected at an appropriate spectral band λ_{em} within the fluorophores' emission spectrum. The interaction of the probe beam with the excited-state molecules at a frequency different from that of their excitation cycle results in a modulation of the residual fluorescence emission at the lasers' cross-correlation frequency, $\Delta\omega = \omega' - \omega$.

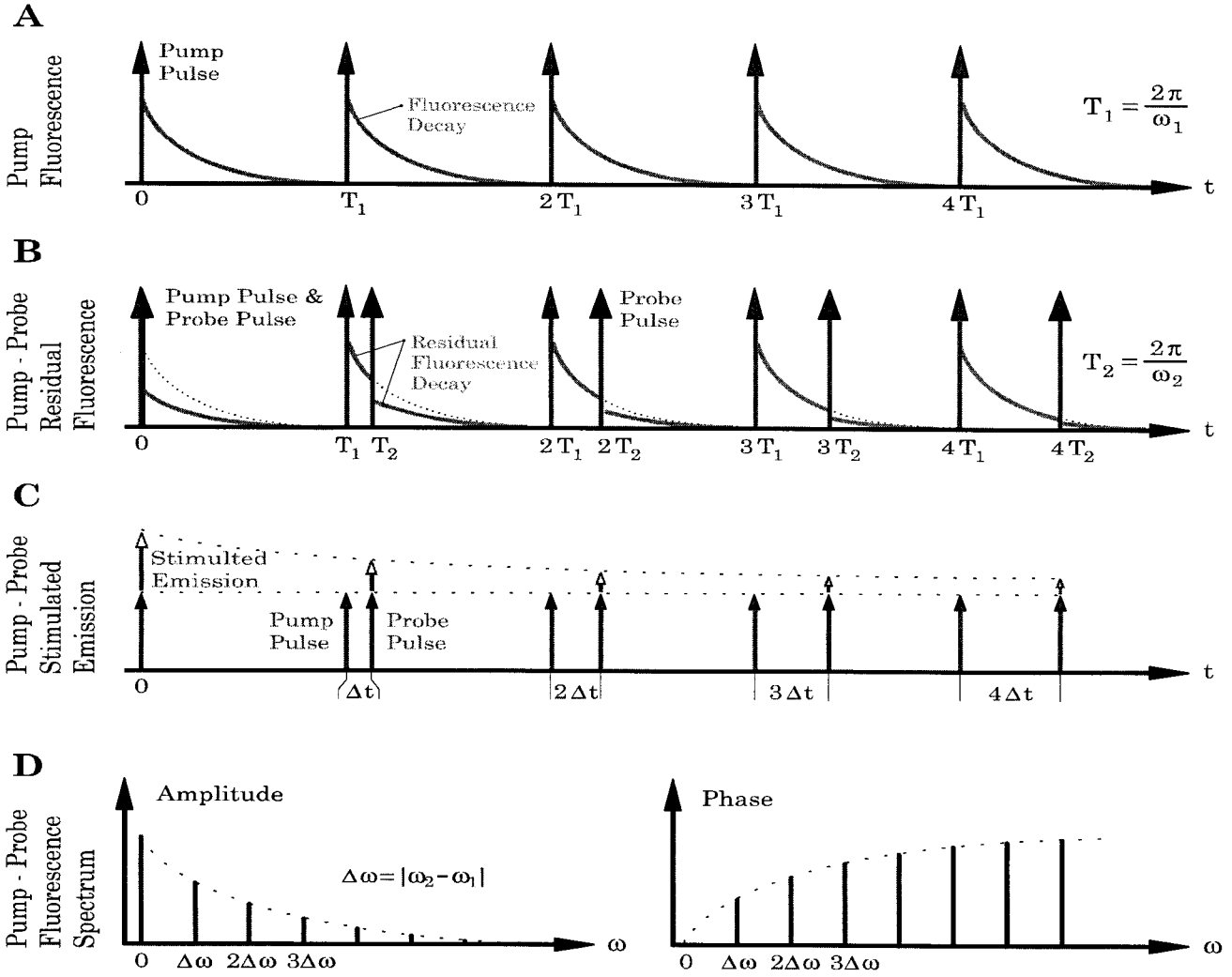

FIGURE 2 Generation of the cross-correlation signal by pulsed lasers. (*A*) Time series of pump laser-induced fluorescence decays. Pump pulses are represented by arrows, at a periodicity of T_1. (*B*) The arrival of probe pulses induces stimulated emission and decreases the residual fluorescence. Probe pulses arrive at a period of T_2. (*C*) The stimulated emission signal (represented by *arrows* above probe pulses) is proportional to the actual number of excited-state molecules. The pump-to-probe pulse delay between consecutive excitation cycles increases by $\Delta t = T_2 - T_1$. (*D*) Fourier transform of the pump-probe stimulated emission signal. $\Delta\omega$ denotes the cross-correlation frequency between the pump and probe lasers.

the chromophores and correspondingly generates a series of fluorescence decays. At increasing numbers of excitation cycles, the probe pulse is successively delayed with respect to the pump pulse. The fundamental delay or an equivalent sampling time is determined by the difference in the lasers' repetition rates. For instance, if the lasers are operated at ~76.2 MHz and the offset frequency is 5 kHz, the equivalent sampling time is ~860 fs. At the arrival of a probe pulse, the correspondingly generated stimulated emission causes a drop in the actual fluorescence because the stimulated emission photons propagate in the same direction as the probe pulse (Sargent et al., 1974). The amplitude of the stimulated emission signal and the drop in fluorescence both depend on the number of excited-state molecules at the arrival time of the probe pulse. As a result, the excited-state population is sampled by the probe pulses at different delays after excitation. The corresponding time-resolved information can be obtained by observing the stimulated emission (same direction as the probe laser) or the residual fluorescence signal emanating in all other directions.

Equations governing the pump-probe stimulated emission process

Our instrument acquires the residual fluorescence intensity $F(t)$ of the pump-probe stimulated emission process. The same objective is used to focus and spatially overlap the two laser beams and to collect the fluorescence (cf. Fig. 4). To obtain an analytical expression for $F(t)$, first consider an

exponentially decaying species that is respectively excited and deexcited (via stimulated emission) by means of a pump and probe laser. The differential equation that governs the number density of excited state chromophores $N(\vec{r}, t)$ now becomes

$$\frac{dN(\vec{r}, t)}{dt} = -\frac{1}{\tau}N(\vec{r}, t) + \sigma I(\vec{r}, t)[c - N(\vec{r}, t)] - \sigma' I'(\vec{r}, t)N(\vec{r}, t) \quad (9)$$

where $I(\vec{r}, t)$ and $I'(\vec{r}, t)$ describe the spatial and temporal intensity distributions of the pump and probe laser, respectively. As in Eq. 1, τ is the fluorophore lifetime, σ is the absorption cross section, and the total fluorophore concentration c is assumed to be constant. The additional term $-\sigma' I'(\vec{r}, t)N(\vec{r}, t)$ accounts for the number of excited-state molecules that return to the ground state via stimulated emission, and σ' denotes the (wavelength-dependent) stimulated emission cross section.

In our experiments the pump and the probe laser generate two periodic pulse trains with slightly different periodicities T and T' or repetition frequencies $\omega = 2\pi/T$ and $\omega' = 2\pi/T'$, respectively. Thus Fourier analysis can be applied to solve Eq. 9. The derivation of an analytical solution of Eq. 9 and, correspondingly, a closed expression for the residual fluorescence $F(t)$ are shown in the Appendix. Here we only present the final expression for the residual fluorescence emission rate $F(t)$ of the pump-probe stimulated emission process (cf. Eq. A8):

$$F(t) = \frac{qc\tau\sigma\sigma'}{2}\sum_{n=0}^{\infty}\frac{L(n\omega)L'(n\omega')}{\sqrt{1 + (n\omega\tau)^2}} \cos[n(\omega' - \omega)t - \phi_n]\int I(\vec{r})I'(\vec{r})d^3\vec{r} \quad (10)$$

In Eq. 10, $L(n\omega)$ and $L'(n\omega)$ are the Fourier coefficients of the temporal pulse profiles $L(t)$ and $L'(t)$ of the pump and probe laser, respectively; q is the quantum yield of the molecules; and the phase shift ϕ_n is given by $\phi_n = \tan^{-1}(n\omega\tau)$.

Both the amplitude $L(n\omega)L'(n\omega')/\sqrt{1 + (n\omega\tau)^2}$ and the phase ϕ_n of each harmonic term contain the fluorescence lifetime τ. For $n = 1$, this result is consistent with Eq. 3. Thus, by measuring the signals' amplitudes and phase spectra at the cross-correlation frequencies, the fluorescence lifetime τ can be determined from $\tan(\phi_n) = n\omega\tau$ and $L(n\omega)L'(n\omega')/\sqrt{1 + (n\omega\tau)^2}$. Note that the high-frequency response is limited by two factors: the harmonic content of the pump and probe laser, respectively, given by $L(n\omega)$ and $L'(n\omega')$, and/or the lifetime modulation factor $\sqrt{1 + (n\omega\tau)^2}$.

Spatial resolution provided by pump-probe fluorescence microscopy

A key feature of the pump-probe method is the localization of the cross-correlation signal within the overlapping integral $\int I(r)I'(r)d^3r$ of the pump and probe beam as shown in Eq. 10. The point-spread function (PSF) of pump-probe techniques has been studied both theoretically and experimentally (Dong et al., 1995, 1997). Spatial specificity is achieved because the pump-probe signal is localized near the focal region where both the pump and probe lasers have a high photon flux. As Eq. 10 shows, in a pump-probe fluorescence microscope in which both the pump and probe processes involve a one-photon transition, the PSF is given by

$$I(r)I'(r) \quad (11)$$

where

$$I(u, v) = \left|2\int_0^1 J_0(v\rho)\rho e^{-(1/2)iu\rho^2}d\rho\right|^2 \quad (12)$$

is the point-spread function for conventional microscopy, $u = (8\pi/\lambda)\sin^2(\alpha/2)z$ and $v = (2\pi/\lambda)\sin(\alpha)r$ are the dimensionless axial (z) and radial (r) coordinates, respectively, and λ is the wavelength of light focused by a circular objective of numerical aperture $\sin(\alpha)$ (Born and Wolf, 1985; Sheppard and Gu, 1990). Equation 12 shows that the PSF is mathematically similar to the PSF of two-photon excitation microscopy $I(u/2, v/2)I(u/2, v/2)$, but at roughly half the wavelength (Sheppard and Gu, 1990). As a result, the PSF of the pump-probe method is narrower than the PSF of two-photon excitation microscopy. Furthermore, the pump-probe PSF is identical to the PSF for confocal microscopy if the stimulated emission wavelength and the confocal detection wavelength are identical. We demonstrated comparable 3-D sectioning effects between pump-probe fluorescence and confocal microscopy (Dong et al., 1995, 1997).

Lifetime and time-resolved polarization imaging in pump-probe stimulated emission microscopy

Fluorescence lifetime measurements are generally performed at the magic angle condition in which the emission polarizer is rotated to 54.7° relative to the excitation beam polarization; the lifetime measured will then be free of the effect due to the chromophores' rotational correlation time. Polarization measurements are achieved by sampling the fluorescence at the parallel and perpendicular directions relative to the polarization of the excitation light source by rotation of the emission polarizer. In the pump-probe (stimulated emission) technique, a different approach is used to satisfy the magic angle and polarization measurement con-

ditions. As illustrated in Fig. 3, the x/z plane polarized pump pulse photoselects those molecules that have their absorption transition dipoles ($\vec{u}_A$) preferentially aligned with the z axis. The polarization of the probe pulse is set at 54.7° relative to that of the pump pulse. Consequently, the resulting modulation of the parallel ($I_\parallel$) and perpendicular ($I_\perp$) fluorescence components is proportional to the numerical factors $\cos^2(54.7°) = 1/3$ and $\sin^2(54.7°) = 2/3$, respectively. Because the fluorescence was detected without an emission polarizer, $I_\parallel$ and $I_\perp$ are acquired at a ratio of 1:2, thus effectively sampling the excited-state molecules at the magic angle. Similarly, to sample the population of the excited-state molecules in directions parallel and perpendicular to the pump beam's polarization, the probe beam's polarization is rotated in parallel and perpendicular directions. Compared to standard fluorescence measurements, the stimulated emission technique samples the distribution of the excited-state molecules by changing the probe beam polarization without the use of an emission polarizer.

Ultrafast molecular dynamics measured without high-speed photodetectors

Direct decay measurements are ultimately limited by the detector frequency response in the study of ultrafast fluorescence phenomena in both the frequency and time domains. A typical photomultiplier (Hamamatsu R928) used in a fluorescence lifetime instrument can be gain-modulated to ~400 MHz. A faster detector such as a microchannel plate has been used up to ~10 GHz (Gratton and vandeVen, 1989). On the other hand, a commonly available laser system can easily generate picosecond pulses (FWHM) corresponding to a 3-dB frequency bandwidth of 220 GHz. Because of the limited detector bandwidth, the standard frequency domain fluorescence instrumentation is not capable of exploring the high modulation frequency content available in picosecond pulsed laser systems. In contrast, pump-probe (stimulated emission) fluorescence microscopy allows lifetime-resolved imaging without the use of fast photodetectors. In Eqs. 3 and 10, we showed that the phase and modulation of the cross-correlation signal at $|\omega' - \omega|$ can be used to determine the fluorescence lifetime. In our experiments, $|\omega' - \omega|$ is chosen in the kHz range, which allows us to acquire images at fast scanning rates.

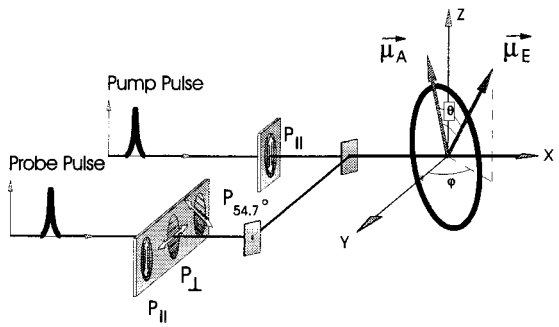

FIGURE 3 Implementation of fluorescence lifetime and anisotropy measurements in the pump-probe (stimulated emission) fluorescence technique. The polarization of the pump pulse ($P_\parallel$) is oriented parallel to the Z axis of the experimental coordinate system. The pump and probe sources are combined and guided to the sample. The fluorescence lifetime is measured with linearly polarized pump and probe pulses. The polarization planes of fluorescence excitation and deexcitation are oriented under the magic angle, i.e., 54.7° ($P_{54.7°}$). The anisotropy is acquired by means of linearly polarized excitation and fluorescence deexcitation parallel ($P_\parallel$) and perpendicular ($P_\perp$) to the excitation. The absorption and emission transition dipoles of a schematically (ellipsoid) represented molecule are denoted as μ_A and μ_E, respectively. The angle θ is between $\vec{\mu}_A$ and $\vec{\mu}_E$, and φ is between the Y axis and the projection of $\vec{\mu}_E$ onto the X/Y plane.

The main focus of this work is to demonstrate that pump-probe stimulated emission microscopy produces time-resolved (in particular, polarization-resolved) images of cells. While we demonstrate the feasibility of this technique, more important biological questions are addressed with appropriate systems. For example, appropriately labeled biomolecules may be introduced into cellular systems, and monitoring the time-resolved polarization properties of these biomolecules can elucidate functionally important motions such as aggregation or change in the local viscosity environment.

MATERIALS AND METHODS

Sample preparation

The two imaging samples presented in this work are orange fluorescent latex spheres and labeled mouse fibroblast cells. Orange fluorescent latex spheres 15 μm in diameter (absorption maximum: 530 nm; emission maximum: 560 nm; Molecular Probes, Eugene, OR) were immobilized between a coverslip and a flat microscope slide with Fluoromount G mounting medium (Southern Biotechnology, Birmingham, AL). The mouse fibroblast cells were grown in Petri dishes on coverslips, using Dulbecco's modified Eagle's medium (DMEM) (D-6655; Sigma, St. Louis, MO) supplemented with 10% fetal bovine serum, 0.11 mg/liter sodium pyruvate, 1% MEM nonessential amino acids, and 0.5% penicillin/streptomycin. CellTracker CMTMR (5-(and 6)-(((4-chloromethyl)benzoyl)amino)tetramethyl-rhodamine (Molecular Probes) was used as the vital fluorescent label. The 1-mg aliquot supplied by the manufacturer was dissolved in dimethyl sulfoxide (DMSO) (Sigma), yielding a 10 mM stock solution. The final dye concentration was 5 μM. For staining, the culture medium was removed from the Petri dish, and the 5 μM CMTMR solution was deposited onto the coverslips' surfaces. After incubating for 30–45 min at 37°C, the coverslips were washed and immersed in fresh culture media and placed back into the incubator for the same period of time. For the microscopic measurements, the coverslips were mounted on well slides filled with the culture medium, and their edges were sealed with nail polish. All measurements were performed at room temperature immediately after the completion of the sealing procedure.

The experimental arrangement of our pump-probe (stimulated emission) fluorescence microscope is shown in Fig. 4. A more comprehensive description of the instrument can be found elsewhere (Dong et al., 1995).

Pump-probe light sources

The 10-MHz output of a master synthesizer is used to synchronize a mode-locked neodymium-YAG laser and a neodymium-YLF laser (Antar-

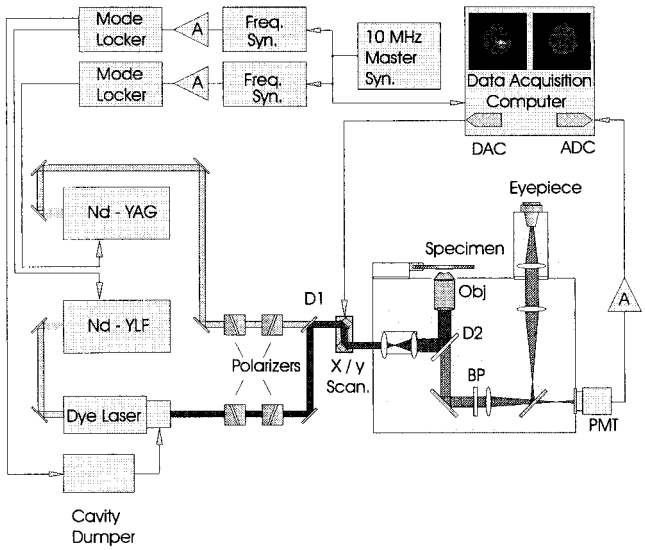

FIGURE 4 Instrumental setup of our pump-probe (stimulated emission) microscope. Nd-YAG and Nd-YLF denote the neodymium-YAG pump and neodymium-YLF probe lasers. D1 and D2 are dichroic mirrors respectively combining and directing the pump and probe beams toward the objective. The spectral properties of D2 are chosen to transmit the fluorescence. BP is the emission bandpass filter that removes residual laser scatter. The fluorescence spot in the specimen plane can be visually inspected through the eyepiece. The fluorescence is recorded by a photomultiplier (PMT). In the imaging mode, the analog PMT signal is first digitized (ADC, analog-to-digital converter) and then acquired by the data acquisition computer. The scanning mirrors of the *X*/*Y* scanner are also computer-driven via a digital-to-analog converter (DAC). In the spectroscopic mode, the PMT signal is recorded by a spectrum analyzer instead of the data acquisition computer (not shown in this figure). Electronic amplifiers are denoted as A.

es; Coherent, Santa Clara, CA). The pulse repetition rate of the two neodymium (Nd) lasers can be separately set by two frequency synthesizers (PTS500; Programmed Test Sources, Littleton, MA). Each PTS synthesizer drives a mode-locker unit and eventually the laser's acousto-optical modulator (not shown in Fig. 4). The (frequency-doubled) 532-nm line of the Nd-YAG laser is used for sample excitation. To induce stimulated emission, the wavelength of the Nd-YLF pumped DCM dye laser (model 700; Coherent) is tuned to 640 nm. The pulse widths (FWHM) of the pump and probe laser are ~100 ps and ~10 ps, respectively. The power and polarization of each laser beam are separately controlled by two Glan-Taylor polarizers (03PTA001; Melles Griot, Irvine, CA). Typically, the average power of the pump and probe beams at the sample plane is less than 300 μW and 3 mW, respectively. For time-resolved fluorescence microscopy, the pump source is operated at 76.2 MHz + 2.5 kHz, and the probe laser's repetition frequency is 5 kHz away at 76.2 MHz + 2.5 kHz. For spectroscopic studies, the difference in repetition frequency is reduced to 210 Hz, with the pump and probe lasers operating at 76.2 MHz and 76.2 MHz + 210 Hz, respectively.

Scanning optics

The two laser beams are combined by a dichroic mirror D1 (Chroma Technology, Brattleboro, VT) before they reach the *x*-*y* scanner (model 6350; Cambridge Technology, Watertown, MA). The angular positions of the two scanning mirrors can be digitally set (DAC) by 16-bit binary numbers. However, only the middle eight bits are used for scanning, correspondingly yielding an image comprising 256 × 256 pixels. The closed-loop bandwidth of the scanner is in the audio range (settling time ~1.6 ms). Therefore, the fastest image acquisition time is ~2 s.

A beam expander is inserted into the microscope's excitation light path to overfill the back-aperture of the objective and hence produce diffraction-limited focusing. The expanded beams are reflected into the microscope objective by a second dichroic D2 (Chroma Technology). We have found that within the angular range used for scanning, the combination of beam expander and objective linearly transforms the angular deviation of the input laser beam into a lateral translation of the focal point position at the object plane. Because the field aperture plane is telecentric to the object plane of the microscope objective, the movement of the focal point on the object plane is proportional to the angular deviation of the scanned beam (Stelzer, 1995).

Because tight focusing increases the photon flux and localizes the pump-probe effect, a well-corrected, high numerical aperture objective is used (63× Plan-Neofluar, NA 1.25; Zeiss, Thornwood, NY). The fluorescence signal is collected by the same objective and transmitted through the dichroic D2 and two bandpass filters BP (600 nm ± 20 nm), before being refocused onto the detector (R3938 or R1104 photomultiplier tube; Hamamatsu, Bridgewater, NJ). For the 63× objective, the scanning range in the object plane is 35 × 35 μm, and the scanning raster is 140 nm.

Signal detection and image processing

For imaging studies, the photomultiplier tube (PMT) signal is first amplified by an ac-coupled (f_{3dB} = 300 Hz) current amplifier (SR570; Stanford Research, Sunnyvale, CA). Then the cross-correlation signal is isolated by a 5 kHz ± 1 kHz bandpass filter and postamplified (SR560, Stanford Research) before its analog-to-digital conversion (ADC) by a 12-bit sampling digitizer (A2D-160; DRA Laboratories, Sterling, VA). The ADC sampling clock is derived from the 10-MHz master line and hence is phase-locked to the lasers. According to the Shannon sampling theorem, at least two points per cross-correlation waveform have to be acquired. In our experiments, the signal is sampled four times per waveform to reduce harmonic noise. To further reduce the noise, several waveforms can be averaged. From such a four-point time record, the phase and amplitude of the 5-kHz cross-correlation signal are derived by fast Fourier transform algorithm. After the predetermined number of waveforms are acquired, the computer correspondingly drives the DAC to advance the scanner to the next pixel. The pixel-to-pixel movement is synchronized to the digitizer for phase coherence. When only one waveform of the 5-kHz cross-correlation signal is acquired, the pixel dwell time is 200 μs, and the corresponding frame acquisition time is 13 s. After digital processing, the amplitude and phase of the cross-correlation signal are displayed and stored by the data acquisition computer. Note that the phase and modulation data are acquired relative to the 10-MHz signal of the master synthesizer. Therefore, a separate measurement with a standard dye is required to calibrate the system.

For spectroscopic studies, the PMT signal is directly acquired by a spectrum analyzer (model 35665A; Hewlett Packard, Rolling Meadows, IL; not shown in the figure). Because of its limited bandwidth (~100 kHz), a smaller cross-correlation frequency is chosen to allow the acquisition of multiple harmonics of a fluorescence decay. The multiharmonic phase and modulation data can be fitted with the appropriate model function to derive the specimen's fluorescence lifetime or rotational correlation time. In contrast to imaging studies that provide only phase and modulation data at a single cross-correlation frequency, a standard dye is therefore not required in the spectroscopic mode. For the saturation studies described in the following section, the cross-correlation signal was set at 210 Hz.

RESULTS AND DISCUSSION

Saturation

We determined the appropriate power levels of the pump and probe lasers to avoid saturation of the cross-correlation signal in the focal region. Initially, the pump-probe (stimulated emission) signal increases linearly as either laser increases in power. With a further increase in the pump and probe laser powers, the ground-state and excited-state populations, respectively, in the focal region can become depleted. Consequently, fluorophores in the off-focal region start to contribute to the pump-probe signal, which results in a broadening of the point-spread function (PSF) and deterioration of image resolution.

As a characteristic fluorophore aqueous rhodamine B (280 μM) was used to determine the appropriate laser intensity values to operate in the linear region. The power levels of both lasers at the objective's focal point were measured by means of a transimpedance amplified solar cell that has been calibrated at the wavelengths of the pump and probe lasers. To mimic data acquisition conditions, the solar cell was placed at the specimen position with a layer of immersion oil between the solar cell and the objective. To enhance the dynamic range of the detection system, off-focal fluorescence was reduced by inserting a 600-μm pinhole at the focal plane of the emission tube lens. For the 63× objective used, the focal volume's radial dimension in the image plane of the tube lens is ~60 μm. Therefore, the 600-μm pinhole only eliminates off-focal fluorescence and does not interfere with the signal from around the focal volume.

For five distinct pump power intensities, i.e., 55, 127, 221, 400, and 510 μW, the first harmonic amplitude at 210 Hz was measured as the probe power was increased stepwise from 860 μW to 7.5 mW. The resulting data series are plotted in Fig. 5 *a*. For each of the five pump power series, the signal amplitude first increases linearly as a function of probe power. However, at higher probe power, the first harmonic amplitude starts to increase at slower rates, indicating the onset of signal saturation. The data series show that probe power saturation begins at ~3 mW regardless of the pump power used. To determine to onset of pump power saturation, the linear region of each data series was fitted. The slopes obtained are plotted in Fig. 5 *b*. Deviation from linearity of the slope indicates the onset of signal saturation due to the pump power level. Therefore, we conclude from Fig. 5 *b* that the signal saturation due to the pump power starts at ~300 μW.

Based on these saturation data, both pump and probe saturation levels of other chromophores can be estimated, provided their extinction coefficients, quantum yields, and stimulated emission cross sections relative to that of rhodamine B are known.

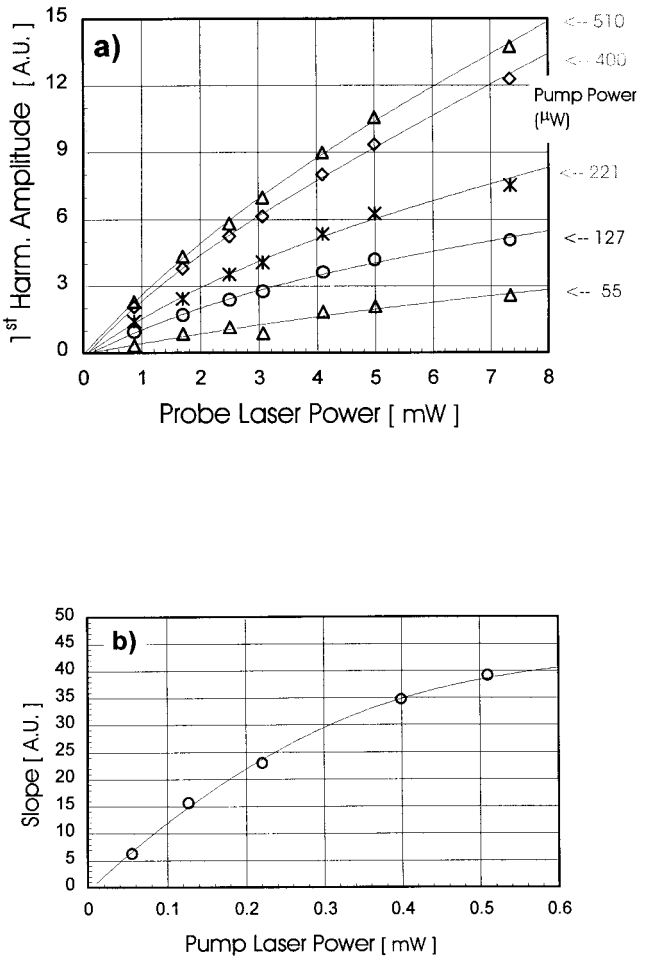

FIGURE 5 (*a*) Cross-correlation signal at different pump and probe laser powers. Data points with equal pump power are connected. (*b*) Slopes obtained from linear regression including only the linear region of the curves in *a*.

Point-spread function

The strong dependence of the optical cross-correlation signal on the spatial overlap of the pump and probe beams provides optical sectioning similar to that found in confocal and two-photon excitation microscopy. For the case of one-photon pump excitation and one-photon probe deexcitation, the point-spread function has been calculated and experimentally verified. It was shown that the radial and axial dimensions of our pump-probe (stimulated emission) microscopy are on the order of 0.3 μm and 1.1 μm, respectively (Dong et al., 1995).

Lifetime and rotation of rhodamine B in water

As an application of the pump-probe (stimulated emission) technique, we measured the lifetime and rotational correlation time of rhodamine B (280 μM) in Tris buffer. The

power spectrum of the fluorescence decay is shown in Fig. 6 *a*. The equivalent (after heterodyning) frequency response of our instrument easily extends into the GHz range, a significant improvement over the 400-MHz limit imposed by PMT modulation in a standard frequency domain fluorometer. Specifically, we can measure harmonics (peaks) of the fluorescence decay of rhodamine B up to 4.572 GHz before the noise significantly distorts the signal.

Because the finite pulse widths of the Nd-YAG and DCM dye lasers cause an attenuation of the high-frequency components, a proper fit of the harmonic decay must include factors accounting for the laser sources' harmonic content. Of course, the Nd-YAG 100-ps pulses ($f_{3db} \approx 2.2$ GHz) contribute more significantly to the high-frequency harmonic distortion than the shorter 10-ps dye laser pulses ($f_{3db} \approx 22$ GHz; cf. Eq. A10).

The appropriate frequency domain fitting function can be derived from Eq. 10 by substituting $L(N\omega)L'(N\omega')$ with the corresponding Fourier coefficients of a Lorentzian-shaped pulse profile (cf. Eq. A11),

$$F(\omega) = \frac{2\pi e^{-b\omega}}{b} \sum_{i=1}^{m} \left[\frac{\alpha_i}{\sqrt{1 + (\omega\tau_i)^2}} \right] \sum_{n=0}^{\infty} \delta(\omega - n\omega_0) \qquad (13)$$

where it is assumed that the fluorescence decay has m components, each one contributing a relative amount α_i.

The corresponding single exponential fit of the data yielded a fluorescence lifetime of 1.54 ns for rhodamine B, in good agreement with the previously measured value of 1.5 ns (Dong et al., 1995). The lifetime fit is shown in Fig. 6 *b*. The factor b was determined to be 61.8 ps, corresponding to a FWHM of 123.6 ps. This value is reasonable because it accounts for both the pulse widths and the relative timing jitter of the two lasers.

Fig. 7 shows the frequency domain differential polarization spectrum of rhodamine B in Tris buffer. The modulation ratio and differential phase were derived from the fluorescence between the parallel and perpendicular orientations of the probe beam with respect to the pump source. Using Globals Unlimited (LFD, Urbana, IL) software, a simple rotator model with a single exponential lifetime of 1.54 ns, and an initial anisotropy of 0.39, the rotational correlation time was determined to be 88 ps. Note that in both the lifetime and rotational measurements, we were able to explore the fluorescence harmonic content up to the GHz range.

Fluorescent latex spheres

To demonstrate the acquisition of time-resolved polarization images, orange fluorescent latex spheres 15 μm in diameter were imaged. For the lifetime-resolved images, the spheres were scanned with the probe beam oriented at 54.7° (magic angle) relative to the pump beam. The first harmonic amplitude and phase data (at 76.2 MHz) of a sphere are

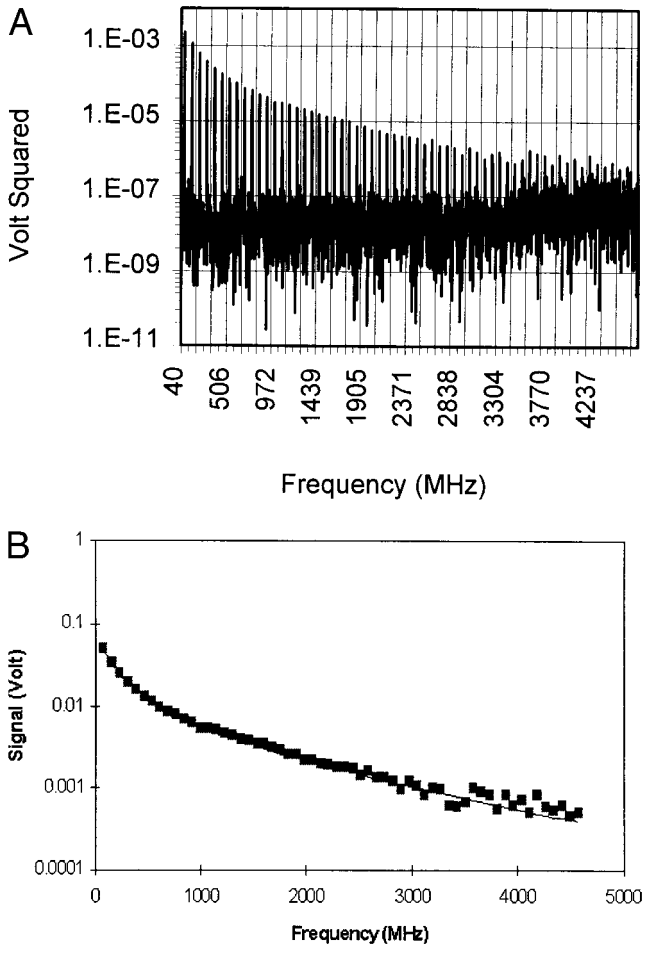

FIGURE 6 (*a*) Power spectrum of aqueous rhodamine B (in Tris). (*b*) Corresponding lifetime fit of the power spectrum data shown in *a*.

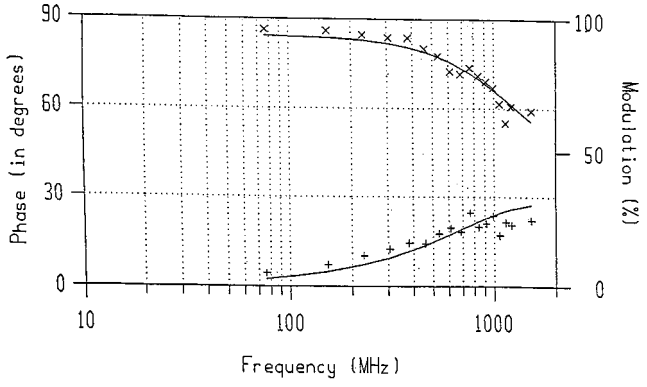

FIGURE 7 Determination of the rotational correlation time of aqueous rhodamine B. The probe beam polarizer is oriented parallel and perpendicular to the pump laser polarization (cf. Fig. 3). The correspondingly measured modulation ratio and differential phase are depicted as × and +, respectively. For a model accommodating a single rotational species, the fit yields a rotational correlation time of 88 ps.

shown in Fig. 8 *a*. The phase values were acquired relative to a reference compound (aqueous rhodamine B, $\tau = 1.5$ ns), a common procedure in phase fluorometry. Within a region inside the sphere (*white square*), the averaged phase is 74.3°. The corresponding fluorescence lifetime of 7.43 ns is derived by means of Eq. 3.

To obtain the time-resolved polarization images, the sphere was scanned twice: first, with the probe beam polarizer oriented parallel (∥) and then perpendicular (⊥) to the pump beam polarization. The first harmonic amplitude and phase data of the polarized images are shown in Fig. 8 *b*. For the same region previously described (*white square*), the averaged phase for parallel excitation and parallel deexcitation (∥/∥) is 68.3°, and that for parallel excitation and perpendicular deexcitation (∥/⊥) is 74.1°. The 5.8° phase shift between the two measurements can be visualized by the histograms of the two phase images also shown in the figure.

The depolarization of fluorescence emission reflected by the phase shift might be caused by energy transfer and/or rotation of dye molecules inside the spheres. To differentiate between the two phenomena, low-temperature (−10°C) fluorescence polarization measurements ($\lambda_{ex} = 532$ nm) of Fluormount G suspended spheres were made in a frequency domain fluorometer (K2; ISS, Champaign, IL). The mea-

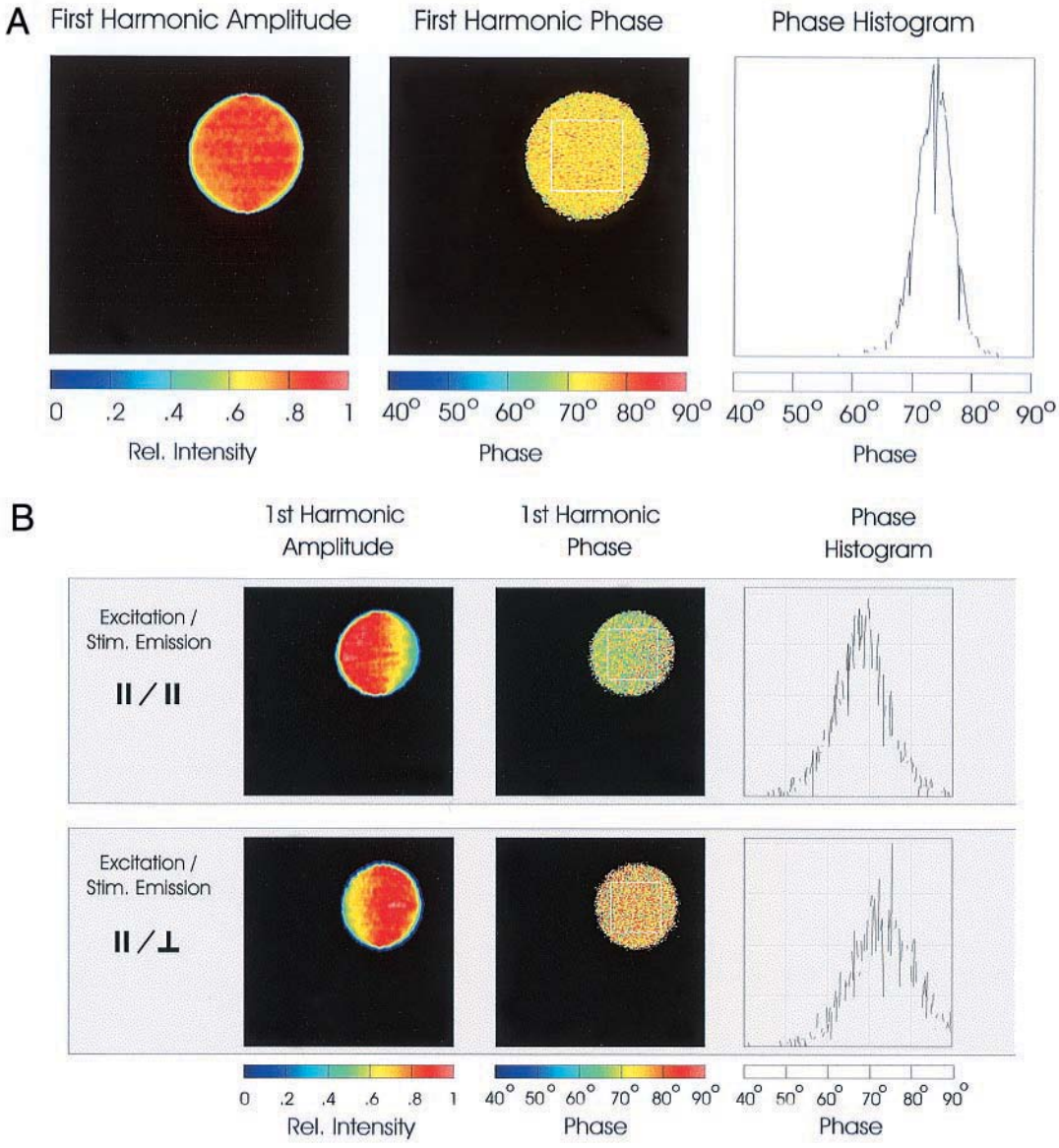

FIGURE 8 (*a*) Lifetime-resolved images of a 15-μm orange fluorescent latex sphere. $\tau_{sphere} = 9.15$ ns (first harmonic amplitude normalized, phase in degrees). (*b*) Time-resolved polarization images of the same sphere. *Top*: First harmonic amplitude and phase image, along with its corresponding phase histogram for ∥-excitation and ∥-deexcitation. *Bottom*: Corresponding data for ∥-excitation and ⊥-deexcitation. Phase difference (derived from *white-bordered region*): $\Delta\varphi = \varphi_{\perp} - \varphi_{\parallel} = 5.8°$.

sured low polarization value of 0.025 indicates that energy transfer is most likely the depolarizing mechanism. In fact, fluorescent spheres from the same manufacturer have been shown to be 95% efficient in excitation transfer efficiency (Roberts et al., 1998).

Mouse fibroblast labeled with CellTracker CMTMR

Using the pump-probe (stimulated emission) microscope, we obtained time-resolved polarization images of mouse fibroblast cells labeled with CellTracker CMTMR (Molecular Probes), a rhodamine based, cell-permeant probe. The CMTMR's chloromethyl group reacts with intracellular thiols. Most likely, the dye enzymatically binds to the glutathione (γ-glutamylcysteinylglycine) commonly found in high concentrations inside cells. The resulting CMTMR-glutathione conjugate is cell-impermeant and is localized primarily in the cell's cytoplasm (Molecular Probes product information sheet).

First, lifetime-resolved amplitude and phase images of a CMTMR-labeled mouse fibroblast were acquired under the magic angle condition. The first harmonic amplitude and phase data (at 76.2 MHz) are shown in Fig. 9 *a*. Again, the phase is determined relative to that of aqueous rhodamine B. The measured phase values are similar (violet-red color) over most of the cell, except for the two distinct regions I and III. For these two areas, the average fluorescence lifetimes are 1.93 ns (region I) and 1.85 ns (region III). For a region in between and an arbitrary chosen area at the top, the lifetime averages are 2.75 ns (region II) and 2.85 ns (region IV).

The first harmonic amplitude is nonuniform across the cell. The variation in amplitude can be due to local changes in both the concentration and the lifetime of fluorophores. From the phase data, it can be seen that the lifetime varies little across the cell. Therefore, the first harmonic amplitude image basically reflects the local concentration of the CMTMR label, except for the two 1.9-ns lifetime regions. The shorter lifetime in these two domains reflects the fact that the CMTMR-glutathione conjugate experiences a microenvironment different from that in the rest of the cell.

Second, time-resolved polarization images of the same mouse fibroblast have been acquired in the same way as previously described (cf. section Fluorescent Latex Spheres). The first harmonic amplitude and phase data are shown in Fig. 9 *b*. The rotational correlation times are derived from both the differential phase and modulation data by means of Eqs. 7 and 8. Assuming r_0 to be 0.39, the rotational correlation times for the same four regions I–VI as marked in the magic angle images (cf. Fig. 9 *a*) are 28, 107, 104, and 151 ps, respectively. The measured rotational rates are fast and correspond roughly to the values obtained for unhindered rotation of small dyes in an aqueous environment. The rotational properties of CMTMR-glutathione conjugate are dominated by CMTMR, because the fluorescent label is about two times larger than glutathione. Because CMTMR is about twice as large as glutathione, such fast rotational correlation times suggest that the cytoplasm acts more like an aqueous than a gel-like environment for the CMTMR-glutathione complex. This is in agreement with recent studies that also used small probes to investigate the microviscosity of the cytoplasm (Periasamy et al., 1991; Swaminathan et al., 1997).

CONCLUSION

We have applied the pump-probe stimulated emission approach to time-resolved polarization imaging. The system has been calibrated for pump-probe signal saturation at both laser powers. Lifetime imaging under the magic angle condition can be satisfied by rotating the probe beam polarization 54.7° relative to that of the pump beam. Similarly, polarization imaging can be achieved by rotating the probe beam polarization parallel and perpendicular to the pump beam. Time-resolved polarization images of fluorescent latex spheres show that the depolarization of fluorescence inside the spheres is most likely due to energy transfer. Lifetime and time-resolved polarization images of CellTracker CMTMR-stained mouse fibroblast cells show fast rotational correlation times of the glutathione-complexed probe ranging from 30 to 150 ps. This implies that a relatively low microviscosity exists inside the cytoplasm.

APPENDIX: DERIVATION OF FREQUENCY DOMAIN, PUMP-PROBE FLUORESCENCE SIGNAL *F(t)*

Based on Eq. 9, we derive an analytical expression for the residual fluorescence intensity $F(t)$ of the pump-probe stimulated emission process. Equation 9 is a first-order linear differential equation of the form $y'(x) + p(x)y = g(x)$, the solution of which is given by

$$y = \frac{1}{\mu(x)}\left[\int^{x} \mu(s)g(s)\mathrm{d}s + c_1\right] \tag{A1}$$

where $\mu(x) = \exp(\int^{x} p(t)\mathrm{d}t)$, and c_1 is a constant specifying the boundary value or initial condition (Boyce and DiPrima, 1977). The solution of Eq. 9 can be written as

$$N(\vec{r}, t) = e^{-\int^{t}[(1/\tau)+\sigma \mathrm{I}(\vec{r}, s)+\sigma' \mathrm{I}'(\vec{r}, s)]\mathrm{d}s}\left[\int^{t} e^{\int^{u}[(1/\tau)+\sigma \mathrm{I}(\vec{r}, s)+\sigma' \mathrm{I}'(\vec{r}, s)]\mathrm{d}s}\sigma c I(\vec{r}, u)\mathrm{d}u\right] \tag{A2}$$

where it is assumed that the excited state is not populated at time zero, i.e., $N(t)|_{t=0} = 0$. According to Fourier theory, the periodic nature of a laser pulse train allows us to write its temporal intensity profile $L(t)$ as a sum of cosines,

$$L(t) = \sum_{n=0}^{\infty} L(n\omega)\cos(n\omega t) \tag{A3}$$

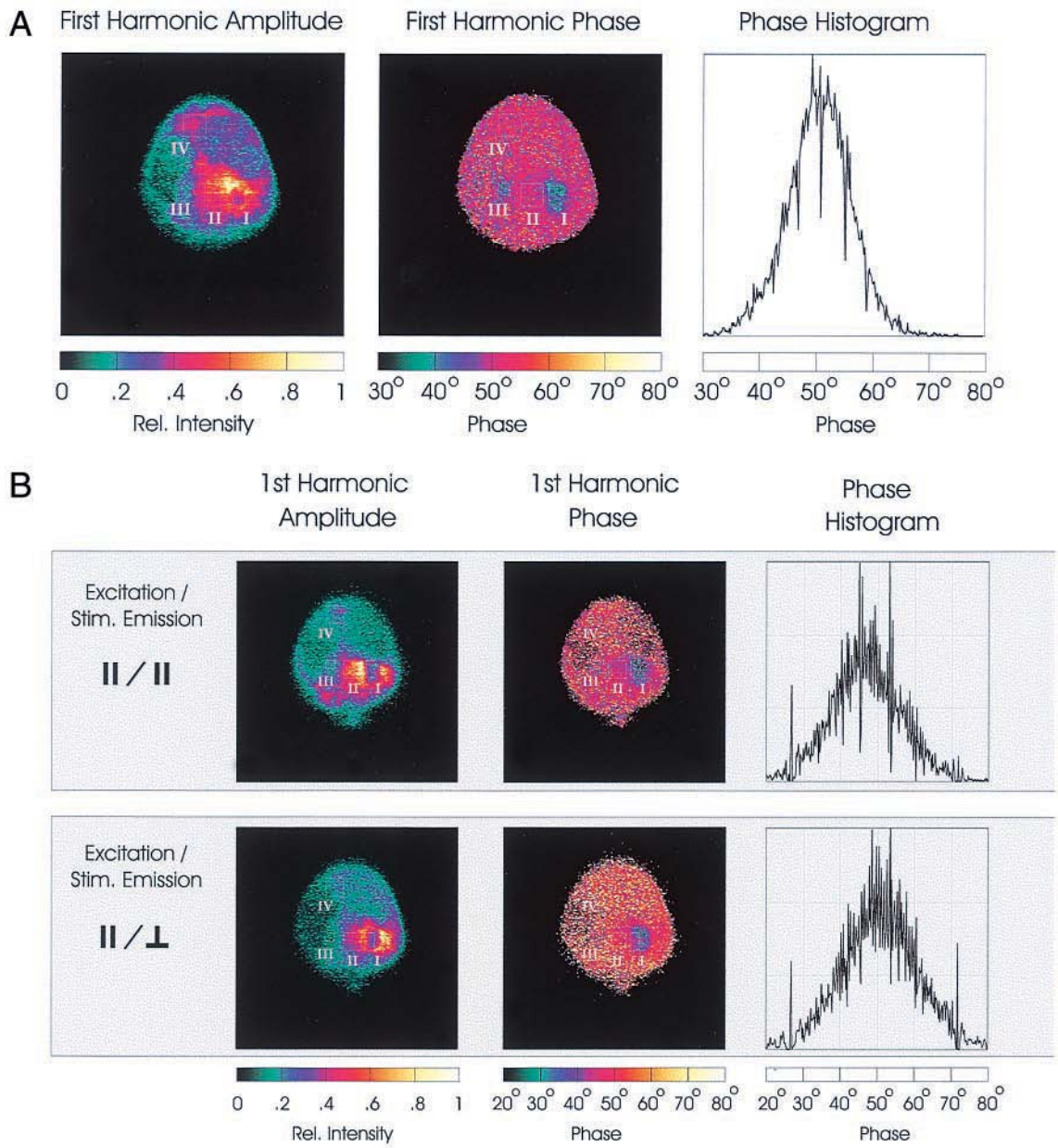

FIGURE 9 (*a*) Lifetime resolved images of a mouse fibroblast cell stained with orange CMTMR (first harmonic amplitude normalized, phase in degrees). The lifetimes derived from regions I–IV are 1.93, 2.75, 1.75, and 2.85 ns, respectively. (*b*) Time-resolved polarization images of the cell in *a*. *Top*: First harmonic amplitude and phase images for ∥-excitation and ∥-deexcitation. *Bottom*: Corresponding data for crossed polarizers. The phase histograms also indicate a shift between ∥- and ⊥-deexcitation. The rotational correlation rates calculated from regions I–IV are 27, 104, 107, and 151 ps, respectively.

where $\omega = 2\pi\nu$ is the angular frequency of the laser pulses, and $L(n\omega)$ is the Fourier coefficient of the nth frequency component of the pulse train. The intensity distribution of a laser pulse train $I(\vec{r}, t)$ focused by a microscope objective can be written as the product of the spatial distribution $I(\vec{r})$ and the temporal profile $L(t)$,

$$I(\vec{r}, t) = I(\vec{r}) \sum_{n=0}^{\infty} L(n\omega)\cos(n\omega t) \qquad \text{(A4)}$$

where the pulse train is assumed to be an even function in time. By substituting the intensity distribution of the pump $I(\vec{r}, t)$ and probe laser $I'(\vec{r}, t)$ according to Eq. A4 into Eq. A2, $N(\vec{r}, t)$ becomes

$$N(\vec{r}, t) = e^{-[(t/\tau)+\sigma I(\vec{r})\Sigma_{k=0}^{\infty}(L(k\omega)/k\omega)\sin(k\omega t)+\sigma' I'(\vec{r})\Sigma_{m=0}^{\infty}(L'(n\omega')/m\omega')\sin(m\omega' t)]}$$

$$\int^{t} e^{-[(u/\tau)+\sigma I(\vec{r})\Sigma_{p=0}^{\infty}(L(p\omega)/p\omega)\sin(p\omega u)+\sigma' I'(\vec{r})\Sigma_{q=0}^{\infty}(L'(q\omega')/q\omega')\sin(q\omega' u)]}\sigma c I(\vec{r})$$

$$\sum_{n=0}^{\infty} L(n\omega)\cos(n\omega u)\mathrm{d}u \qquad \text{(A5)}$$

The instantaneous fluorescence emission rate $F(\vec{r}, t)$ is the product of the molecules' quantum yield q and the rate of change of the excited-state population,

$$F(\vec{r}, t) = -q \frac{\mathrm{d}N(\vec{r}, t)}{\mathrm{d}t}. \tag{A6}$$

Evaluation of Eq. A6 with the result of Eq. A5 yields

$$\begin{aligned} F(\vec{r}, t) = -q\sigma c I(\vec{r}) \Bigg\{ & \sum_{\mathrm{N}=0}^{\infty} L(N\omega)\cos(N\omega t) \\ & - \Bigg(\frac{1}{\tau} + \sigma I(\vec{r}) \sum_{\mathrm{n}=0}^{\infty} L(n\omega)\cos(n\omega t) + \sigma' I'(\vec{r}) \\ & + \sigma' I'(\vec{r}) \sum_{\mathrm{m}=0}^{\infty} L'(m\omega')\cos(m\omega' t) \Bigg) \\ & e^{-((\mathrm{t}/\tau)+\sigma \mathrm{I}(\vec{\mathrm{r}})\Sigma_{\mathrm{n}=0}^{\infty}\mathrm{L}(\mathrm{n}\omega)\cos(\mathrm{n}\omega\mathrm{t})+\sigma' \mathrm{I}'(\vec{\mathrm{r}})\Sigma_{\mathrm{m}=0}^{\infty}\mathrm{L}(\mathrm{m}\omega')\cos(\mathrm{m}\omega'\mathrm{t}))} \\ & \sum_{\mathrm{n}=0}^{\infty} L(n\omega) \int^{\mathrm{t}} e^{\mathrm{u}/\tau} e^{\sigma \mathrm{I}(\vec{\mathrm{r}})\Sigma_{\mathrm{p}=0}^{\infty}(\mathrm{L}(\mathrm{p}\omega)/\mathrm{p}\omega)\sin(\mathrm{p}\omega\mathrm{t})+\sigma \mathrm{I}(\vec{\mathrm{r}})\Sigma_{\mathrm{q}=0}^{\infty}(\mathrm{L}(\mathrm{q}\omega)/\mathrm{q}\omega)\sin(\mathrm{q}\omega' \mathrm{t})} \\ & \cos(n\omega u)\mathrm{d}u \Bigg\} \end{aligned} \tag{A7}$$

Equation A7 can be simplified. The exponentials containing sinusoidal functions may be expanded and the integral evaluated. The resulting first-order cross-correlation term in $I(\vec{r})I'(\vec{r})$ for the fluorescence emission rate is

$$\begin{aligned} F(t) = \frac{qc\tau\sigma\sigma'}{2} & \sum_{\mathrm{n}=0}^{\infty} \frac{L(n\omega)L'(n\omega')}{\sqrt{1 + (n\omega\tau)^2}} \\ & \cos[n(\omega' - \omega)t - \phi_{\mathrm{n}}] \int I(\vec{r})I'(\vec{r})\mathrm{d}^3\vec{r} \end{aligned} \tag{A8}$$

where $\tan(\phi_{\mathrm{n}}) = n\omega\tau$ (cf. Eq. 3).

The Fourier coefficients $L(n\omega)$ and $L'(n\omega')$ depend on the shape of the pump and probe laser pulses, respectively. For mode-locked lasers like those used in our setup, the temporal intensity profile $L(t)$ can be approximated as a train of Lorentzian-shaped pulses with a FWHM $\Delta t = 2b$ and a period of T (Alcala and Gratton, 1985):

$$L(t) = \sum_{\mathrm{n}=-\infty}^{\infty} 1/[b^2 + (t - nT)^2] \tag{A9}$$

The corresponding frequency domain representation is given by

$$L(\omega) = \frac{\pi e^{-\mathrm{b}\omega}}{b} \sum_{\mathrm{n}=0}^{\infty} \delta(\omega - n\omega_0) \tag{A10}$$

with $\omega_0 = 2\pi/T$. The -3-dB frequency bandwidth is $f_{3\mathrm{db}} = \ln 2/(\pi\Delta t)$. (For 10-ps pulses, for instance, $f_{3\mathrm{db}}$ is ~22 GHz.) Thus the nth frequency component of a Lorentzian-shaped laser pulse train is

$$L(n\omega) = \frac{\pi e^{-\mathrm{b}\omega}}{b} \delta(\omega - n\omega) \tag{A11}$$

(Alcala and Gratton, 1985).

We thank Dr. Matt Wheeler's group for providing us with mouse fibroblast cells.

This work was supported by the National Institutes of Health (RR03155).

REFERENCES

Adachi, S., S. Takeyama, and Y. Takagi. 1995. Dual wavelength optical sampling technique for ultrafast transient bleaching spectroscopy. *Opt. Commun.* 117:71–77.

Alcala, J. R., and E. Gratton. 1985. A multifrequency phase fluorometer using the harmonic content of a mode-locked laser. *Anal. Instrum.* 14:225–250.

Berland, K. M., E. Gratton, and M. J. vandeVen. 1992. A laser heterodyning detector for frequency domain ultrafast spectroscopy. Time-resolved laser spectroscopy in biochemistry III. *SPIE Proc.* 1640:370–378.

Betzig, E., R. J. Chichester, F. Lanni, and D. L. Taylor. 1993. Near-field fluorescence imaging of cytoskeletal actin. *Bioimaging.* 1:129–135.

Boyce and DiPrima. 1977. Elementary Differential Equations and Boundary Value Problems, 3rd Ed. John Wiley and Sons, New York.

Born, M., and E. Wolf. 1985. Principles of Optics, 5th Ed. Pergamon Press, Oxford.

Buurman, E. P., R. Sanders, A. Draaijer, H. C. Gerritsen, J. J. F. Van Veen, P. M. Houpt, and Y. K. Levine. 1992. Fluorescence lifetime imaging using a confocal laser scanning microscope. *Scanning.* 14:155–159.

Christov, I. P., V. Stoev, M. M. Murnane, and H. C. Kapteyen. 1996. Sub-10-fs operation of Kerr-lens mode-locked lasers. *Opt. Lett.* 21: 1493–1495.

Denk, W., J. H. Strickler, and W. W. Webb. 1990. Two-photon laser scanning fluorescence microscopy. *Science.* 248:73–76.

Dix, J. A., and A. S. Verkman. 1990. Pyrene excimer mapping in cultured fibroblasts by ratio imaging and time-resolved microscopy. *Biochemistry.* 29:1949–1953.

Dong, C. Y., P. T. C. So, C. Buehler, E. Gratton. 1997. Spatial resolution in scanning pump-probe fluorescence microscopy. *Optik J. Light Electron Opt.* 106:7–14.

Dong, C. Y., P. T. C. So, T. French, and E. Gratton. 1995. Fluorescence lifetime imaging by asynchronous pump-probe microscopy. *Biophys. J.* 69:2234–2242.

Draaijer, A., R. Sanders, and H. C. Gerritsen. 1995. Fluorescence lifetime imaging, a new tool in confocal microscopy. *In* Handbook of Biological Confocal Microscopy. J. Pawley, editor. Plenum Press, New York. 491–505.

Elzinga, P. A., R. J. Kneisler, F. E. Lytle, G. B. King, and N. M. Laurendeau. 1987. Pump/probe method for fast analysis of visible spectral signatures utilizing asynchronous optical sampling. *Appl. Opt.* 26: 4303–4309.

Elzinga, P. A., F. E. Lytle, Y. Jian, G. B. King, and N. M. Laurendeau. 1987. Pump/probe spectroscopy by asynchronous optical sampling. *Appl. Spectrosc.* 41:2–4.

Evans, D. K., editor. 1989. Laser Applications in Physical Chemistry. Marcel Dekker, New York.

Fleming, G. R. 1986. Chemical Applications of Ultrafast Spectroscopy. Oxford University Press, New York.

Fushimi, K., and A. S. Verkman. 1991. Low viscosity in the aqueous domain of cell cytoplasm measured by picosecond polarization microfluorimetry. *J. Cell Biol.* 112:719–725.

Gratton, E., D. M. Jameson, and R. D. Hall. 1984. Multifrequency phase and modulation fluorometry. *Annu. Rev. Biophys. Bioeng.* 13:105–124.

Gratton, E., and M. Limkeman. 1983. A continuously variable frequency cross-correlation phase fluorometer with picosecond resolution. *Biophys. J.* 44:315–324.

Gratton, E., and M. vandeVen. 1989. A superheterodyning microwave phase fluorometer with femtosecond resolution. LFD Report 18.

Hochstrasser, R. M., and C. K. Johnson. 1988. Biological processes studied by ultrafast laser techniques. *In* Ultrashort Laser Pulses. W. Kaiser, editor. Springer-Verlag, New York. 357–417.

Kao, H. P., J. R. Abney, and A. S. Verkman. 1993. Determinants of the translational mobility of a small solute in cell cytoplasm. *J. Cell Biol.* 120:175–184.

Keating, S. M., and T. G. Wensel. 1990. Nanosecond fluorescence microscopy: emission kinetics of Fura-2 in single cells. *Biophys. J.* 59:186–202.

Koenig, K., and H. Schneckenburger. 1994. Laser-induced autofluorescence for medical diagnosis. *J. Fluorescence.* 4:17–40.

Kusba, J., V. Bogdanov, I. Gryczynski, and J. R. Lakowicz. 1994. Theory of light quenching: effects on fluorescence polarization, intensity, and anisotropy decays. *Biophys. J.* 67:2024–2040.

Lakowicz, J. R. 1999. Principles of Fluorescence Spectroscopy. Kluwer Academic and Plenum Press, New York.

Lakowicz, J. R., I. Gryczynski, V. Bogdanov, and J. Kusba. 1994. Light quenching and fluorescence depolarization of rhodamine B. *J. Phys. Chem.* 98:334–342.

Lytle, F. E., R. M. Parrish, and W. T. Barnes. 1985. An introduction to time-resolved pump/probe spectroscopy. *Appl. Spectrosc.* 39:444–451.

Morgan, C. G., A. C. Mitchell, and J. G. Murray. 1991. Prospects for confocal imaging based on nanosecond fluorescence decay time. *J. Microsc.* 165:49–60.

Periasamy, N., M. Armijo, and A. S. Verkman. 1991. Picosecond rotation of small polar fluorophores in the cytosol of sea urchin eggs. *Biochemistry.* 30:11836–11841.

Piston, D. W., D. R. Sandison, and W. W. Webb. 1992. Time-resolved fluorescence imaging and background rejection by two-photon excitation in laser scanning microscopy. *SPIE Proc.* 1640:379–389.

Roberts, D. V., B. P. Wittmerhaus, Y. Z. Zhang, S. Swan, and M. P. Klinkosky. 1998. Efficient excitation energy transfer among multiple dyes in polystyrene microspheres. *J. Luminescence.* 79:225–231.

Sargent, M., III, M. O. Scully, and W. E. Lamb, Jr. 1974. Laser Physics. Addison-Wesley Publishing Company, London.

Schneckenburger, H., P. Gessler, and I. Pavenstadt-Grupp. 1992. Measurement of mitochondrial deficiencies in living cells by microspectrofluorometry. *J. Histochem. Cytochem.* 40:1573–1578.

Schneckenburger, H., and K. Koenig. 1992. Fluorescence decay kinetics and imaging of NAD(P)H and flavins as metabolic indicators. *Opt. Eng.* 31:1447–1451.

Sheppard, C. J. R., and M. Gu. 1990. Image formation in two-photon fluorescence microscopy. *Optik.* 86:104–106.

So, P. T. C., T. French, W. M. Yu, K. M. Berland, C. Y. Dong, and E. Gratton. 1996. Two-photon fluorescence microscopy: time-resolved and intensity imaging. *In* Fluorescence Imaging Spectroscopy and Microscopy. X. F. Wang and B. Herman, editors. John Wiley and Sons, New York. 351–374.

Spencer, R. D., and G. Weber. 1969. Measurements of subnanosecond fluorescence lifetimes with a cross-correlation phase fluorometer. *Ann. N.Y. Acad. Sci.* 158:361–376.

Stelzer, E. H. K. 1995. The intermediate optical system of laser-scanning confocal microscopes. *In* The Handbook of Biological Confocal Microscopy. J. Pawley, editor. Plenum Press, New York. 139–153.

Swaminathan, R., C. P. Hoang, and A. S. Verkman. 1997. Photobleaching recovery and anisotropy decay of green fluorescent protein GFP-S65T in solution and cells: cytoplasmic viscosity probed by green fluorescent protein translational and rotational diffusion. *Biophys. J.* 72:1900–1907.

Voss, E. 1990. Anti-fluorescein antibodies as structure-function models to examine fundamental immunological and spectroscopic principles. *Comm. Mol. Cell Biophys.* 6:197–221.

Wilson, T., editor. 1990. Confocal Microscopy. Academic Press, London.

Wilson, T., and C. Sheppard. 1984. Theory and Practice of Scanning Optical Microscopy. Academic Press, London.

Xu, L., D. Spielmann, F. Krausz, and R. Szipocs. 1996. Ultrabroadband ring oscillator for sub-10-fs pulse generation. *Opt. Lett.* 21:1259–1261.

Zhou, J., G. Taft, C. P. Huang, I. P. Christov, H. C. Kapteyn, and M. M. Murnane. 1994. Sub-10 fs pulse generation in Ti:sapphire: capabilities and ultimate limits. *In* Ultrafast Phenomena IX. P. F. Barbara, W. H. Knox, G. A. Mourou, and A. H. Zewail, editors. Springer-Verlag, Berlin. 39–40.